

UNDERSTANDING THE GROWTH DYNAMICS Cs₃Sb THIN FILMS VIA IN-SITU CHARACTERIZATION TECHNIQUES: TOWARDS EPITAXIAL ALKALI ANTIMONIDE PHOTOCATHODES*

A. Galdi[†], C. T. Parzyck, W. J. I. DeBenedetti, J. Balajka, L. Cultrera, I. V. Bazarov, H. Paik, L. Moreschini, C. Hu, K. M. Shen, M. A. Hines, J.M. Maxson
Cornell University, Ithaca, NY, USA

Abstract

Alkali antimonide photocathodes, such as Cs₃Sb, have attractive properties, such as low emittance and high quantum efficiency, which makes them excellent candidates for next-generation high-brightness electron sources. A large number of studies in literature focus on quantum efficiency and lifetime, and fewer report chemical and structural analysis, despite the latter ultimately determine the brightness at the photocathode. Epitaxial, single-crystalline films would allow to study the intrinsic properties of alkali antimonide photocathodes and to optimize them for maximum brightness, but this goal remains elusive. A strong limiting factor is the extreme air sensitivity, preventing ex-situ structural and chemical analysis. We used vacuum suitcase transfer to study the morphology of Cs₃Sb samples grown on different substrates with scanning tunneling microscopy. Samples grown on SiC substrates show 10 times larger islands than samples grown on other substrates in the same conditions. Further studies with *in situ* reflection high energy electron diffraction demonstrate favorable growth dynamics on SiC, making it a preferable substrate for epitaxial growth of Cs₃Sb.

INTRODUCTION

The performance of many types of linear accelerators, such as energy recovery linacs [1], high repetition rate free electron lasers [2] and ultrafast electron diffraction beam-lines [3], depends on the initial brightness of the electron beam generated by the photocathode. The normalized 5D brightness B_n photoemission source (the photocathode) is defined as:

$$B_n = \frac{2m_e c^2 I}{\sigma_x^2 \text{MTE}}, \quad (1)$$

where m_e is the electron mass, c the speed of light, I the beam current, σ_x the rms beam size at the cathode and MTE is the mean transverse energy of the photoemitted electrons. For pulsed beams $B_n \propto E_0^n / \text{MTE}$, where E_0 is the electric field at the cathode (or launch field) and $n=1.5-2$ depending on the regime [4]. Hence, using low MTE photocathodes in high gradient photoinjectors is highly desirable. Cs₃Sb photocathodes achieve low MTE when operated at low temperature and near the photoemission threshold, for example MTE as low as 22 meV was measured at 90 K with 690 nm

photon excitation [5]. However typical Cs₃Sb photocathodes are characterized by a disordered structure with rough surface [6]. Surface roughness contributes to the initial momentum spread of electrons, resulting in an enhancement to MTE: $\Delta_{\text{MTE}} \propto E_0$ [7, 8].

For this reason, controlling the surface roughness is an important area of research for this class of photocathode materials [9]. One possible approach to roughness reduction is pursuing epitaxial growth of Cs₃Sb on suitable single crystal substrates, keeping in mind that important requisites to select a substrate are not only the geometrical similarity between the film and substrate surfaces, but also the surface stability and chemical compatibility [10].

We started by testing different single crystalline substrates by growing Cs₃Sb by codeposition on them, and by using the quantum efficiency (QE, i.e the number of photoemitted electrons per incident photon) of the photocathode at 505 nm as feedback during the growth, as described in refs [11, 12].

We selected the following substrates: Al₂O₃(10 $\bar{1}$ 0) ($a_1 = 0.4758$ nm, $a_2 = 1.299$ nm), rutile TiO₂(001) ($a_{\text{TiO}_2} = 0.4594$ nm), cubic SiC (3C-SiC)(100) ($a_{\text{SiC}} = 0.4397$ nm); Cs₃Sb has a cubic structure with lattice parameter $a = 0.9147$ nm (close to twice the SiC and TiO₂ ones). Al₂O₃ has in-plane lattice parameters close to 1/2 and 4/3 of the Cs₃Sb, but the structure of the (10 $\bar{1}$ 0) surface, on closer inspection, does not offer a regular template for the growth of a cubic FCC structure like Cs₃Sb.

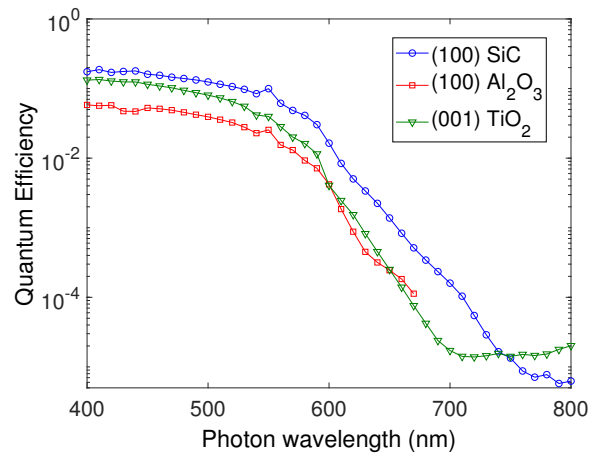


Figure 1: Spectral response of Cs₃Sb photocathodes grown on different substrates, showing excellent photoresponse independently from the substrate material.

* This work was supported by the U.S. National Science Foundation under Awards OIA-1549132, the Center for Bright Beams, and PHYS-1535279.
[†] ag733@cornell.edu

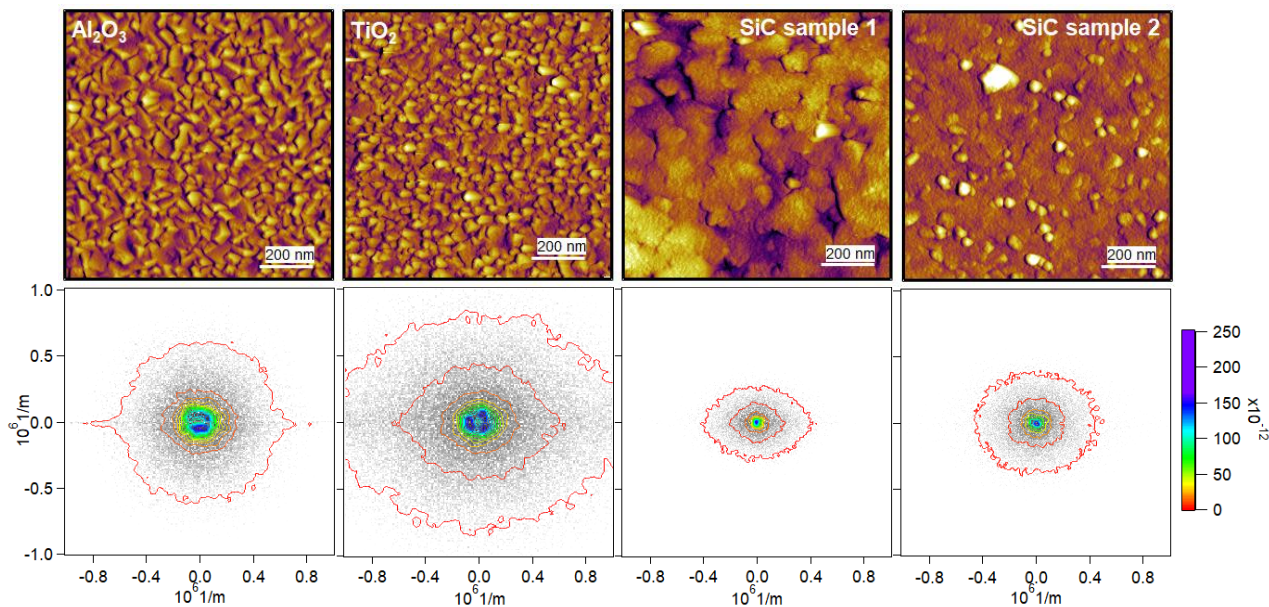


Figure 2: Top: STM images of samples grown on different substrates. Bottom: absolute value of the Fourier coefficients plotted versus the corresponding spatial frequency (gray scale); contour lines are obtained by 5x5 smoothing. The two outermost contours correspond to 5×10^{-12} m and 1×10^{-12} m respectively.

RESULTS

In Fig. 1 we report the spectral responses of a series of Cs_3Sb samples grown consecutively in the same conditions on different substrates (substrate temperature 70°C , Cs flux 1×10^{13} atoms/cm²/s) [11], showing excellent photoresponse independently from the substrate material. The sample grown on 3C-SiC has a slightly lower photoemission threshold. The samples were transferred from the growth system to a UHV scanning tunneling microscopy (STM) system using a vacuum suitcase [12]. In the top panel of Fig. 2 we report STM images of the 3 samples of Fig. 1 and of a replicated sample on SiC (SiC#2). The images represent the STM tip displacement $z(x, y)$ while scanning the sample surface (x, y) using as feedback the tunnel current between the tip (grounded) and the sample (biased at 0.85-1 V). The tunnel current depends both on the tip-sample distance and on the local density of states, and it is kept constant during the measurement; given the order of the recorded tip displacement, we attribute them to the sample morphology, and use them to estimate the surface roughness and its contribution to MTE. We calculated the rms roughness σ_r by averaging the standard deviation of $z(x, y)$ on images of different size (1000×1000 nm² and 500×500 nm²), and we report the results in Table 1. The samples grown on SiC have lower σ_r , though of the same order of magnitude of the other samples.

However, the samples on SiC have much larger islands than the samples grown on different substrates (about $\times 10$). In the bottom panel of Fig. 2 we report the modulus of

Table 1: rms Value of the Surface Roughness and Roughness Contribution to MTE Calculated as Described in the Text

SAMPLE	σ_r (nm)	Δ_{MTE}/E_0 (meV/MV·m)
Al_2O_3	2.4	1.06
TiO_2	2.95	4.02
SiC#1	2.06	0.24
SiC#2	1.73	0.79

the coefficients of the Fourier decomposition of $z_0(x, y) = z(x, y) - \langle z \rangle$ versus the corresponding spatial frequency; it is evident that the surface of the samples grown on SiC are described by smaller spatial frequencies. The surface roughness contribution to MTE, in the limit of small kinetic energy of the photoelectrons, is due to the distortion of the electric field by the rough surface, that causes the electrons to acquire additional transverse velocity [13]. We calculated the roughness contribution to MTE per unit MV/m, Δ_{MTE}/E_0 , using the method described in refs [7, 14] on the height data of Fig. 2 with 40 to 50 independent frequencies. Our calculations suggest a substantial decrease of the roughness contribution to emittance due to the large island size achieved on 3C-SiC(100) substrates.

The samples appear composed by disordered grains, but we are unable to verify if they have indeed a completely disordered crystal structure or if some crystal order is realized in some of the samples. For this reason we performed

further experiments at the thin film growth user facility of the PARADIM project (Cornell University). This gave us access to a molecular beam epitaxy (MBE) system equipped with reflection high energy electron diffraction (RHEED) and a series of advanced characterization techniques, such as angle resolved photoemission spectroscopy, x-ray photoelectron spectroscopy, low energy electron diffraction. RHEED consists in electron diffraction that uses an electron beam with a 10-15 kV energy incident at a glancing angle ($0.5 - 6^\circ$) on the sample to create a diffraction pattern on a fluorescent screen. The RHEED is typically installed in MBE systems to provide real-time diagnostic during growth [15].

In Fig. 3 we show the RHEED patterns of two samples grown via codeposition on 3C-SiC(100) substrates. The pattern of Fig. 3(a1) corresponds to a sample grown while the substrate was cooling from heat cleaning at 650°C , at a thermocouple temperature of $30-40^\circ\text{C}$. The QE measured at the end of the growth at 504 nm was $\sim 10\%$. The pattern consists in concentric rings that are obtained when the electron beam transmits through disordered grains with random orientation. The pattern is transformed in radial coordinates and the radial coordinate is converted to the electron scattering vector; the angle-integrated intensity is shown by lines in Fig. 3(a2), and compared to the calculated x-ray diffraction pattern of Cs_3Sb as reported by the ICSD card #44714. Transmission patterns are observed on rough samples (i.e. like the samples shown in Fig. 2) where the electron beam passes through the grains instead of being reflected on the surface of the sample. If the sample was fully disordered, i.e. the grain orientation was completely random, the intensity of the rings would be uniform. In our case the rings present bright and dark spots, indicating some partial preferential orientation of the grains, i.e. a texture. By rotating the sample around its surface normal, we observed the spots moving on the ring circumference, indicating that the texture axis is in the sample plane [16]. For comparison, samples grown on Si(100) in similar conditions do not show any texture, but rather uniform intensity rings.

The sample of Fig. 3(b1) is grown at higher temperature (108°C) and characterized by a QE of $\sim 2 \times 10^{-5}$. The pattern consists in streaks, meaning that the sample is flat enough that the electron beam is reflected by the sample and sees only the in-plane periodicity of the sample surface [15]. In this case the streaks do not change when rotating the sample, indicating that the sample has a single crystalline axis oriented along the surface normal and random orientation of the in-plane crystalline axes [16]. We can distinguish two sets of equally spaced streaks. In Fig. 3(b2) we plot the scattering vector versus the streak index measured from the central specular streak for the two sets of streaks. This allows to determine two in plane lattice parameters: $d_1 = 7.08 \pm 0.04 \text{ \AA}$ and $d_2 = 5.6 \pm 0.1 \text{ \AA}$. These lattice parameters do not find correspondence in the Cs_3Sb structure, indicating that we are stabilizing a different phase of the Cs-Sb system [17]. Similar RHEED pattern and lattice parameters are observed for films grown at $T \geq 95^\circ\text{C}$ on 3C-SiC(100) and $\text{TiO}_2(110)$ substrates.

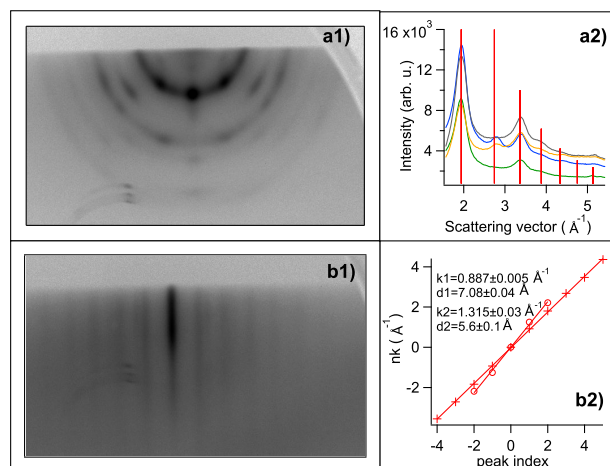


Figure 3: (a1) RHEED pattern of a Cs-Sb sample grown on 3C-SiC(100) at a temperature of about $30-40^\circ\text{C}$. (a2) Diffracted intensity versus scattering vector for RHEED patterns collected at different azimuths. Vertical bars correspond to the calculated diffraction pattern of Cs_3Sb , based on ICSD database. (b1) RHEED pattern of a Cs-Sb sample grown on 3C-SiC(100) at a temperature of about 108°C . (b2) Linear fits of scattering vector as a function of peak index for the two sets of streaks observed in (b1).

CONCLUSIONS

We have studied the structure of Cs-Sb codeposited thin films grown on different substrates with different techniques (STM and RHEED). Samples grown on 3C-SiC(100) show larger islands than samples grown on different substrates, that would result in better performance in high gradient photoinjectors. RHEED reveals partial ordering of the crystal structure on 3C-SiC(100) substrates and the possibility of stabilizing different phases of the Cs-Sb system by varying the substrate temperature during growth.

ACKNOWLEDGEMENTS

This work was supported by the U.S. National Science Foundation under Award PHY-1549132, the Center for Bright Beams and by the National Science Foundation (Platform for the Accelerated Realization, Analysis, and Discovery of Interface Materials (PARADIM)) under Cooperative Agreement No. DMR-1539918.

REFERENCES

- [1] M. A. H. Schmeißer *et al.*, "Towards the operation of Cs-KSb photocathodes in superconducting RF photoinjectors," *Phys. Rev. Accel. Beams*, vol. 21, p. 113401, Nov. 2018. doi:10.1103/PhysRevAccelBeams.21.113401
- [2] P. Musumeci *et al.*, "Advances in bright electron sources," *Nucl. Instrum. Methods Phys. Res., Sect. A*, vol. 907, pp. 209–220, 2018. doi:10.1016/j.nima.2018.03.019
- [3] H. Lee, X. Liu, L. Cultrera, B. Dunham, V. O. Kostroun, and I. V. Bazarov, "A cryogenically cooled high voltage dc

- photoemission electron source,” *Rev. Sci. Instrum.*, vol. 89, no. 8, p. 083303, 2018. doi:10.1063/1.5024954
- [4] J. Rosenzweig *et al.*, “Ultra-high brightness electron beams from very-high field cryogenic radiofrequency photocathode sources,” *Nucl. Instrum. Methods Phys. Res., Sect. A*, vol. 909, pp. 224–228, 2018. doi:10.1016/j.nima.2018.01.061
- [5] L. Cultrera, S. Karkare, H. Lee, X. Liu, I. Bazarov, and B. Dunham, “Cold electron beams from cryocooled, alkali antimonide photocathodes,” *Phys. Rev. Spec. Top. Accel. Beams*, vol. 18, no. 11, p. 113401, 2015. doi:10.1103/PhysRevSTAB.18.113401
- [6] S. Schubert *et al.*, “Bi-alkali antimonide photocathodes for high brightness accelerators,” *APL Mater.*, vol. 1, no. 3, p. 032119, 2013. doi:10.1063/1.4821625
- [7] J. Feng, S. Karkare, J. Nasiatka, S. Schubert, J. Smedley, and H. Padmore, “Near atomically smooth alkali antimonide photocathode thin films,” *J. Appl. Phys.*, vol. 121, no. 4, p. 044904, 2017. doi:10.1063/1.4974363
- [8] S. Karkare and I. Bazarov, “Effect of nanoscale surface roughness on transverse energy spread from GaAs photocathodes,” *Appl. Phys. Lett.*, vol. 98, no. 9, p. 094104, 2011. doi:10.1063/1.3559895
- [9] J. Xie *et al.*, “Synchrotron x-ray study of a low roughness and high efficiency K₂CsSb photocathode during film growth,” *J. Phys. D: Appl. Phys.*, vol. 50, no. 20, p. 205303, 2017. doi:10.1088/1361-6463/aa6882
- [10] J. T. Paul, A. Galdi, C. Parzyck, K. Shen, and R. G. Hennig, “Computational synthesis of substrates by crystal cleavage,” arXiv:2002.00903v3
- [11] A. Galdi *et al.*, “The effects of oxygen-induced phase segregation on the interfacial electronic structure and quantum efficiency of Cs₃Sb photocathodes,” *J. Chem. Phys.*, vol. 153, no. 14, p. 144705, 2020. doi:10.1063/5.0024020
- [12] A. Galdi *et al.*, “Towards the optimization of photocathode properties via surface science techniques: A study on Cs₃Sb thin film growth,” in *Proc. North American Particle Accelerator Conf. (NAPAC’19)*, Lansing, MI, USA, Sep. 2019, paper MOPLH24.
- [13] D. J. Bradley, M. B. Allenson, and B. R. Holeman, “The transverse energy of electrons emitted from GaAs photocathodes,” *J. Phys. D: Appl. Phys.*, vol. 10, no. 1, pp. 111–125, Jan. 1977. doi:10.1088/0022-3727/10/1/013
- [14] T. Gorlov, “High-precision calculation of quasistatic field near a photocathode surface microrelief,” *J. Electrostat.*, vol. 65, no. 12, pp. 735–741, 2007. doi:10.1016/j.elstat.2007.05.010
- [15] S. Hasegawa, “Reflection high-energy electron diffraction,” in *Characterization of Materials*, Hoboken, NJ, USA: Wiley, 2012, pp. 1–14.
- [16] D. Litvinov, T. O’Donnell, and R. Clarke, “In situ thin-film texture determination,” *J. Appl. Phys.*, vol. 85, no. 4, pp. 2151–2156, 1999. doi:10.1063/1.369519
- [17] J. Sangster and A. D. Pelton, “The Cs-Sb (cesium-antimony) system,” *J. of Phase Equilibria*, vol. 18, pp. 382–386, 1997. doi:10.1007/s11669-997-0065-z